nanomaterials

MDPI

Communication

Facile Synthesis of Hierarchical $CoSeO_3 \cdot 2H_2O$ Nanoflowers Assembled by Nanosheets as a Novel Anode Material for High-Performance Lithium-Ion Batteries

Xiao-Xu Ji [1], Qing-Huai Zhao [1], Hao Chen [2], Xin-Wei Luo [2], Yi Shang [2] and Xiao-Di Liu [2,*]

[1] College of Physics and Electronic Engineering, Nanyang Normal University, Nanyang 473061, China; xxji2010@163.com (X.-X.J.); zqh1262022@126.com (Q.-H.Z.)
[2] College of Chemistry and Pharmaceutical Engineering, Nanyang Normal University, Nanyang 473061, China; xiaohao819@126.com (H.C.); 17527755065@163.com (X.-W.L.); s3030199101@163.com (Y.S.)
* Correspondence: 20122029@nynu.edu.cn

Abstract: As novel anodic materials for lithium-ion batteries (LIBs), transitional metal selenites can transform into metal oxide/selenide heterostructures in the first cycle, which helps to enhance the Li^+ storage performance, especially in terms of high discharge capacity. Herein, well-defined hierarchical $CoSeO_3 \cdot 2H_2O$ nanoflowers assembled using 10 nm-thick nanosheets are successfully synthesized via a facile one-step hydrothermal method. When used as anodic materials for LIBs, the $CoSeO_3 \cdot 2H_2O$ nanoflowers exhibit a considerably high discharge capacity of 1064.1 mAh g^{-1} at a current density of 0.1 A g^{-1}. In addition, the obtained anode possesses good rate capability and cycling stability. Owing to the superior electrochemical properties, the $CoSeO_3 \cdot 2H_2O$ nanoflowers would serve as promising anodic materials for high-performance LIBs.

Keywords: hydrothermal method; $CoSeO_3 \cdot 2H_2O$; nanoflowers; nanosheets; lithium-ion batteries

Citation: Ji, X.-X.; Zhao, Q.-H.; Chen, H.; Luo, X.-W.; Shang, Y.; Liu, X.-D. Facile Synthesis of Hierarchical $CoSeO_3 \cdot 2H_2O$ Nanoflowers Assembled by Nanosheets as a Novel Anode Material for High-Performance Lithium-Ion Batteries. *Nanomaterials* **2022**, *12*, 2474. https://doi.org/10.3390/nano12142474

Academic Editor: Cheol-Min Park

Received: 8 June 2022
Accepted: 18 July 2022
Published: 19 July 2022

1. Introduction

With the increasing demands of portable electronics and electric vehicles, lithium-ion batteries (LIBs) with high power density and good cycle stability urgently need to be developed [1–4]. The commercial graphite anodic material is limited to acquiring the requirement of high power density owing to its low theoretical capacity (372 mAh g^{-1}) [5,6]. Thus, much effort has been made to explore novel and effective anodes for high-performance LIBs.

In the last few years, transitional metal selenides have received considerable attention for their rich redox active sites, high electronic conductivity, and large theoretical capacities, thus leading to superior electrochemical performance. Accordingly, transitional metal selenides are promising anodes of LIBs [7–10]. On the other hand, heterostructures composed of materials with different bandgaps can form an internal electric field at the heterointerface, resulting in facilitated charge transport and enhanced surface reaction kinetics [11–15]. For instance, SnS/SnO_2 can form an electric field in the nanocrystal, so they possess much lower ion-diffusion resistance and accordingly exhibit outstanding high-rate capability and good cycle stability [14]. Therefore, constructing metal-selenide-based heterostructures would endow them with fascinating electrochemical performance. Fortunately, it has been found that cobalt selenites can transform into cobalt oxide and cobalt selenides in the initial charge/discharge processes and form metal oxide/selenide heterostructures. In these regards, cobalt selenites can be used as ideal and effective anodic materials for high-performance LIBs.

Nevertheless, cobalt selenites still suffer from pulverization due to the large volume change during the charge and discharge processes, leading to rapid capacity decay [16]. It is confirmed that the rational design of the structure of cobalt selenites is a practical strategy to overcome this problem [17–19]. For example, Jiang et al. prepared metastable $CoSeO_3 \cdot H_2O$

nanosheets, which could exhibit reversible capacities of 1100 and 515 mAh g^{-1} at 3 and 10 A g^{-1} after 1000 cycles, respectively [17]; anhydrous $CoSeO_3$ porous microspheres were shown to be capable of delivering a high reversible capacity of 709 mAh g^{-1} after 1400 cycles at a current density of 3 A g^{-1} [16]. It is well-known that the morphologies of nanomaterials are dominated by the crystalline structure of initial seeds and external factors. As one kind of cobalt selenite, $CoSeO_3 \cdot 2H_2O$, has a different crystal structure from other cobalt selenites [17,20,21]. Thus, it is reasonable to consider that $CoSeO_3 \cdot 2H_2O$ with a unique morphology would be obtained by rational design, and accordingly, the electrochemical performance would be improved. However, the synthesis and Li^+ storage properties of $CoSeO_3 \cdot 2H_2O$ have not been reported.

Recently, 3D hierarchical nanostructures assembled from low-dimensional building blocks have attracted tremendous attention in the field of LIBs [22]. As is known to all, 3D hierarchical nanostructures can not only provide large contact areas between the electrode and electrolyte, but also accommodate volume change and accelerate Li^+ transport [23]. Hence, it is urgent to explore novel and effective methods for preparing hierarchical $CoSeO_3 \cdot 2H_2O$ nanostructures to achieve the goals of high capacity and long life.

Herein, we report a simple and effective one-step hydrothermal method for the synthesis of hierarchical $CoSeO_3 \cdot 2H_2O$ nanoflowers for the first time. The $CoSeO_3 \cdot 2H_2O$ nanoflowers were assembled using nanosheets with thickness of ~10 nm. Owing to the unique structure, the obtained $CoSeO_3 \cdot 2H_2O$ nanoflowers exhibited high specific capacity, superior rate capability, and excellent cycling stability.

2. Materials and Methods

2.1. Synthesis of Hierarchical $CoSeO_3 \cdot 2H_2O$ Nanoflowers

All the chemicals were purchased from Shanghai Aladdin Bio-Chem Technology Co. Ltd. and used without purification. $Co(CH_3COOH)_2 \cdot 4H_2O$ (0.2491 g) and $Na_2SeO_3 \cdot 5H_2O$ (0.1315 g) were dissolved into a mixed solvent of 10 mL deionized water and 5 mL ammonium hydroxide (80%) and stirred for 10 min. Then, the obtained solution was transferred into an autoclave and heated at 150 °C for 12 h. After the reaction, the product was washed with deionized water and ethanol. After dried at 80 °C for 10 h, hierarchical $CoSeO_3 \cdot 2H_2O$ nanoflowers were obtained.

2.2. Structural Characterizations

The crystalline structure of the product was analyzed using an X-ray diffractometer (XRD, Rigaku D/max-2500, Rigaku Corporation, Tokyo, Japan) using Cu Kα radiation. The morphology, nanostructure, and composition of the sample were characterized using field emission scanning electron microscopy (FESEM, JEOL JSM-6700F, JEOL Ltd., Akishima, Tokyo, Japan), transmission electron microscopy (TEM, JEOL JEM-2010, JEOL Ltd., Japan), and high-resolution TEM (HRTEM, JEOL JEM-2010, JEOL Ltd., Japan).

2.3. Electrochemical Performance Measurement

Hierarchical $CoSeO_3 \cdot 2H_2O$ nanoflowers (70 wt%), carbon black (20 wt%), and polyvinylidene fluoride (PVDF, 10 wt%) were mixed into N-methyl-2-pyrrolidone to form a slurry, which was then uniformly coated on copper foils and dried at 120 °C for 12 h in vacuum to generate working electrodes. The loading amount of the electrode was about 2 mg cm^{-2}. 1 mol L^{-1} $LiPF_6$ dissolved in ethylene carbonate (EC) and diethyl carbonate (DC) (1:1 by volume) was employed as the electrolyte. Li foil and polypropylene membrane were chosen as the counter electrode and separator, respectively. Then, the CR2025 button batteries were assembled in an argon-filled glovebox. The LAND CT2001A battery tester (Shenglan Electronic Technology Co., Ltd, Dongguan, China) was used to evaluate the electrochemical properties of the obtained anode.

3. Results

The XRD pattern of the sample is shown in Figure 1a. All diffraction peaks match well with monoclinic $CoSeO_3 \cdot 2H_2O$ with space group of $P2_1/n(14)$ and lattice parameters of a = 6.5151 Å, b = 8.8253 Å, and c = 7.6404 Å (JCPSD No. 52-0215). The diffraction peaks at 15.48°, 25.71°, 29.60°, 32.73°, 35.81°, 37.83°, 40.95°, and 52.78° can be indexed to the (011), (012), (210), (031), (12−2), (113), (040), and (313) facets, respectively. Clearly, no other crystal phases (e.g., $CoSe_2$, Co_3O_4) can be found, which reveals the high purity of the sample.

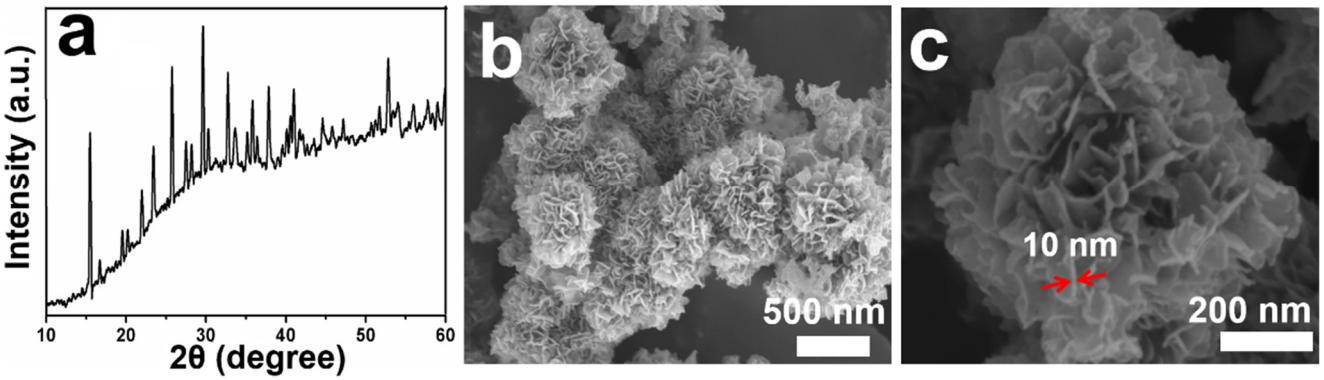

Figure 1. (**a**) XRD pattern, (**b**,**c**) FESEM images of the $CoSeO_3 \cdot 2H_2O$ nanoflowers.

The morphologies of the products were analyzed using FESEM, and the results are shown in Figure 1b,c. As can be seen from Figure 1b, the obtained products are consisted of nanoscale flower-like $CoSeO_3 \cdot 2H_2O$. As shown in the high-magnification FESEM image (Figure 1c), the $CoSeO_3 \cdot 2H_2O$ nanoflowers are made up of numerous ultrathin nanosheets with thicknesses of ~10 nm (marked by the red arrows). In the synthesis, $CoSeO_3 \cdot 2H_2O$ nuclei prefer to grow into ultrathin nanosheets owing to their anisotropic crystal characteristics. Thus, in the following growth process, to minimize the surface energies, these primary nanosheets have a strong tendency to interconnect with each other and form into 3D hierarchical nanoflowers with obviously open structure. This special hierarchical structure can accelerate the diffusion of Li^+, provide more areas for the contact between electrode and electrolyte, and alleviate the volume changes during the charge/discharge processes, thus leading to enhanced electrochemical performance [24,25].

As shown in Figure 2, the nanostructures of the as-obtained $CoSeO_3 \cdot 2H_2O$ nanoflowers were studied using TEM analysis. The different magnification TEM images (Figure 2a,b) can further prove that the samples are hierarchical nanoflowers assembled with ultrathin nanosheets. The HRTEM image (Figure 2c) shows the typical lattice spacing of 0.238 nm (marked by yellow dotted box), which agrees with the (113) facets of monoclinic $CoSeO_3 \cdot 2H_2O$. In addition, the element distribution of the $CoSeO_3 \cdot 2H_2O$ nanoflowers were investigated using STEM (Figure 2d), coupled with EDX mapping (Figure 2e–g). Clearly, the Co, Se, and O elements are homogeneously distributed in the $CoSeO_3 \cdot 2H_2O$ nanoflowers, coinciding with the above XRD result (Figure 1a).

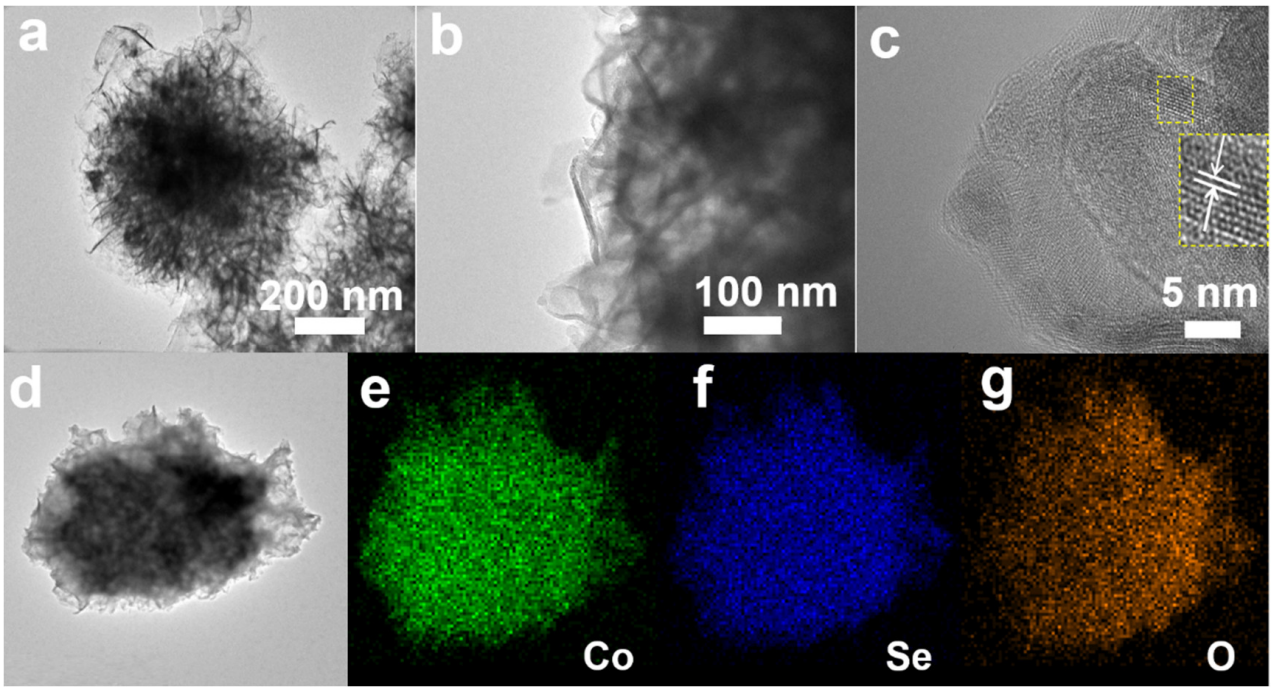

Figure 2. (**a**,**b**) TEM images, (**c**) HRTEM image, and (**d**) STEM image of the $CoSeO_3 \cdot 2H_2O$ nanoflowers; (**e**–**g**) EDX mapping images of Co, Se, and O.

The electrochemical properties of the obtained $CoSeO_3 \cdot 2H_2O$ anode were researched through the galvanostatic method. Figure 3a shows the first, second, and third charge–discharge curves of the hierarchical $CoSeO_3 \cdot 2H_2O$ nanoflower anodes in the voltage range of 0.01–3.0 V (vs. Li^+/Li) at a current density of 0.1 A g^{-1}. The initial discharge and charge capacities are 1064.1 and 897.3 mAh g^{-1}, respectively, and the coulombic efficiency and the irreversible capacity of the first cycle is 84.3% and 166.8 mAh g^{-1}. The capacity loss may be attributed to the formation of Li_2O by intercalated Li^+ and SEI film owing to the decomposition of electrolyte during the first cycle on the electrode surface [17]. In the following second and third cycles, the coulombic efficiency is 95.7% and 97%, respectively, which indicates the good reversibility of the $CoSeO_3 \cdot 2H_2O$ anode.

The rate capability of the $CoSeO_3 \cdot 2H_2O$ electrode was studied by progressively increasing the current densities from 0.1 to 0.2, 0.5, 1.0, and 2 A g^{-1}. As shown in Figure 3b, the discharge capacity of the $CoSeO_3 \cdot 2H_2O$ nanoflowers gradually decreases from 1058.9 to 858.1, 816.7, 765.5 and 678.6 mAh g^{-1} when increasing the current density from 0.1 to 0.2, 0.5, 1.0 and 2.0 A g^{-1}, respectively. Importantly, the discharge capacity is still as high as 678.6 mAh g^{-1} as the current density is increased to 2.0 A g^{-1}. Then, the discharge capacity can return to 762.7 mAh g^{-1} as the current density is reduced to 1 A g^{-1}. The above results suggest the excellent structural stability at high current density and superior rate performance of the anode.

Besides the rate capability, the cycling performance of the $CoSeO_3 \cdot 2H_2O$ electrode was also evaluated at a constant current density of 0.5 A g^{-1} for 180 cycles, and the result is shown in Figure 3c. As can be clearly seen, the curve is almost a straight line, and the electrode can retain a high reversible capacity of 626 mAh g^{-1} after 180 cycles. Meanwhile, the high coulombic efficiency of 98% can be obtained in the subsequent cycles after the first few cycles, which further indicates the excellent cyclic stability of the $CoSeO_3 \cdot 2H_2O$ electrode. Figure S1 is the FESEM image of the $CoSeO_3 \cdot 2H_2O$ electrode after the cyclic stability test. Obviously, the hierarchical structure of the sample can be maintained even after long and intensive battery operation, suggesting the excellent electrochemical stability. In addition, the discharge capacity of the electrode is slightly increased from the first to the fiftieth cycle and then slowly decreased during the following cycles, which may be attributed to the

gradual electrolyte penetration and the reversible growth of the electrochemistry active polymeric gel-like film by the activated electrolyte degradation [26,27]. Compared to other Co, Se-based anodes materials [12,28–35], the $CoSeO_3 \cdot 2H_2O$ nanoflowers exhibit better electrochemical performance (Table S1), suggesting their promising application in energy storage devices.

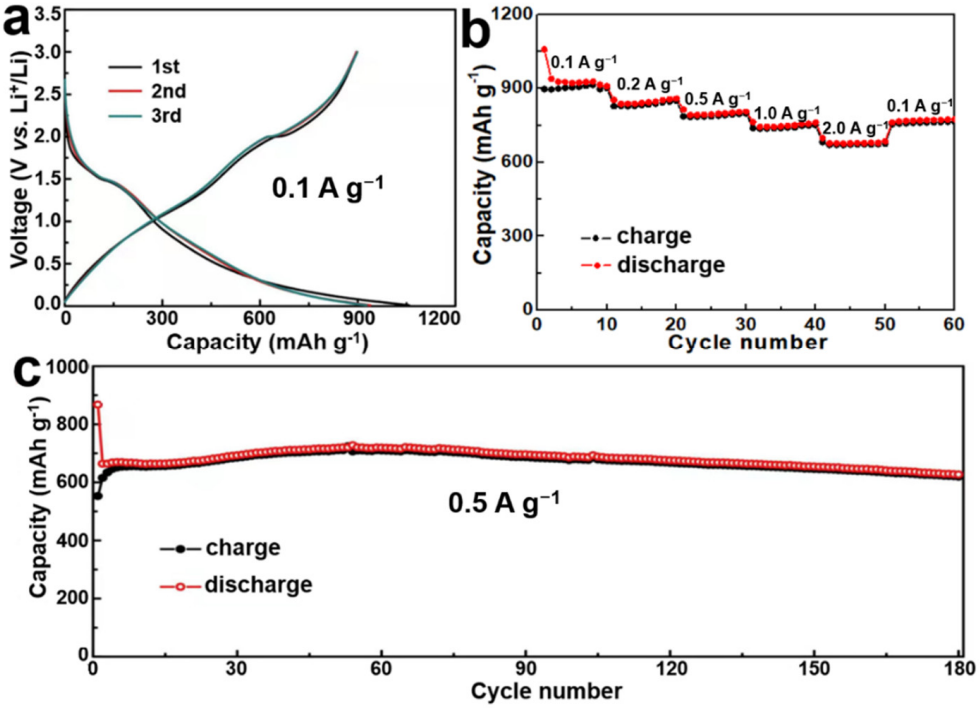

Figure 3. Electrochemical properties of the $CoSeO_3 \cdot 2H_2O$ nanoflowers: (**a**) charge-discharge curves for the first three cycles at a current density of 0.1 A g^{-1}; (**b**) rate capability at various current densities; (**c**) cycling performance at 0.5 A g^{-1}.

Based on some important literature [17,18,36], $CoSeO_3 \cdot 2H_2O$ can be converted into CoO and SeO_2 during the first discharge and charge processes. In the following lithiation and delithiation procedures, the reversible reaction mechanism of CoO and SeO_2 with Li^+ ions can be described by the reaction (Equation (1)):

$$CoO + xSeO_2 + (1 - x)Se + 4(x + 1)Li^+ + 4(x + 1)e^- \leftrightarrow Co + (2x + 1)Li_2O + Li_2Se. \quad (1)$$

In order to better comprehend the Li^+-ions storage mechanism of $CoSeO_3 \cdot 2H_2O$, some analysis methods, such as in situ EIS, in situ XRD, ex suit XPS, ex suit TEM, and so on, can be further conducted [36,37]. On the other hand, to deeply research the relationship between nanostructure and performance, it is appropriate to fabricate other control samples in the future. In addition, it is worth mentioning that the improvement of low-temperature performance is very important for next-generation LIBs [38]; furthermore, size reduction, doping, and surface modification are potential methods for enhancing the low-temperature performance of electrodes [39,40]. Hence, it is reasonable to consider that many efforts should be made to the controlled synthesis of $CoSeO_3 \cdot 2H_2O$ with other morphologies, heteroatoms doped $CoSeO_3 \cdot 2H_2O$, and $CoSeO_3 \cdot 2H_2O$@C composites.

4. Conclusions

In summary, $CoSeO_3 \cdot 2H_2O$ nanoflowers were successfully synthesized using an effective and simple hydrothermal method for the first time. When used as the anode materials for LIBs, the $CoSeO_3 \cdot 2H_2O$ electrodes exhibited excellent Li^+ storage properties, which can be attributed to the hierarchical flower-like architecture and the open structure. The

present method is expected to be extended to the synthesis of other metal selenites with unique morphologies and improved properties.

Supplementary Materials: The following supporting information can be downloaded at: https://www.mdpi.com/article/10.3390/nano12142474/s1, Figure S1: FESEM image of the $CoSeO_3 \cdot 2H_2O$ electrode after 180 cycles at 0.5 A g^{-1}; Table S1: The comparison of the electrochemical performance the $CoSeO_3 \cdot 2H_2O$ nanoflowers and other previously reported Co,Se-based anodes for LIBs. References [12,28–35] are cited in the Supplementary Materials.

Author Contributions: Original draft preparation, writing X.-X.J.; review and editing, X.-D.L. and Q.-H.Z.; experiment, H.C. and X.-W.L.; analysis Y.S. All authors have read and agreed to the published version of the manuscript.

Funding: This research was funded by the National Natural Science Foundation of China (No. 51802163). This research was also funded by the Training Program for Young Backbone Teachers of the Education Department of Henan Provincial (No. 2020GGJS182).

Data Availability Statement: Data presented in this article are available at request from the corresponding author.

Conflicts of Interest: The authors declare no conflict of interest.

References

1. Li, Y.; Kong, L.B.; Liu, M.C.; Zhang, W.B. One-step synthesis of micro/nano flower-like $Ni_3V_2O_8$ as anode for Li-ion batteries. *Mater. Letter.* **2017**, *186*, 289–292. [CrossRef]
2. Qin, C.L.; Zheng, D.H.; Hu, Q.F.; Zhang, X.M.; Wang, Z.F.; Li, Y.Y.; Zhu, J.S.; Ou, J.Z.; Yang, C.H.; Wang, Y.C. Flexible integrated metallic glass-based sandwich electrodes for high-performance wearable all-solid-state supercapacitors. *Appl. Mater. Today* **2020**, *19*, 100539. [CrossRef]
3. Bruce, P.G.; Scrosati, B.; Tarascon, J.M. Nanomaterials for rechargeable lithium batteries. *Angew. Chem. Int. Ed.* **2008**, *47*, 2930–2946. [CrossRef] [PubMed]
4. Armand, M.; Tarascon, J.M. Building better batteries. *Nature* **2008**, *451*, 652–657. [CrossRef]
5. Etacheri, V.; Marom, R.; Elazari, R.; Salitra, G.; Aurbach, D. Challenges in the development of advanced Li-ion batteries: A review. *Energy Environ. Sci.* **2011**, *4*, 3243. [CrossRef]
6. Tarascon, J.M.; Armand, M. Issues and challenges facing rechargeable lithium batteries. *Nature* **2010**, *414*, 359–367. [CrossRef]
7. Wei, Z.X.; Wang, L.; Zhuo, M.; Ni, W.; Wang, H.X.; Ma, J.M. Layered tin sulfide and selenide anode materials for Li- and Na-ion batteries. *J. Mater. Chem. A* **2018**, *6*, 12185–12214. [CrossRef]
8. Wang, L.; Wang, Z.H.; Xie, L.L.; Zhu, L.M.; Cao, X.Y. An enabling strategy for ultra-fast lithium storage derived from microflower-structured NiX (X=O, S, Se). *Electrochim. Acta* **2020**, *343*, 136138. [CrossRef]
9. Li, J.; Liu, W.; Chen, C.; Zhao, X.X.; Qiu, Z.Z.; Xu, H.M.; Sheng, F.; Hu, Q.F.; Zheng, Y.; Lin, M.; et al. High yield electrochemical exfoliation synthesis of tin selenide quantum dots for high-performance lithium-ion batteries. *J. Mater. Chem. A* **2019**, *7*, 23958–23963. [CrossRef]
10. Liang, T.; Wang, H.W.; Wang, R.; He, B.B.; Gong, Y.S.; Yan, C.J. Nitrogen-doped carbon nanotube-buffered $FeSe_2$ anodes for fast-charging and high-capacity lithium storage. *Electrochim. Acta* **2021**, *389*, 138686. [CrossRef]
11. Liu, Q.; Hou, J.G.; Hao, Q.H.; Huang, P.; Xu, C.C.; Zhou, Q.X.; Zhou, J.; Liu, H. Nitrogen-doped carbon encapsulated hollow ZnSe/$CoSe_2$ nanospheres as high performance anodes for lithium-ion batteries. *Nanoscale* **2020**, *12*, 22778–22786. [CrossRef] [PubMed]
12. Hao, Q.Y.; Cui, G.L.; Zhao, Y.; Bakenov, Z. Flower-Like $MoSe_2/MoO_2$ composite with high capacity and long-term stability for lithium-ion battery. *Nanomaterials* **2019**, *9*, 1256. [CrossRef] [PubMed]
13. Rivest, J.B.; Jain, P.K. Cation exchange on the nanoscale: An emerging technique for new material synthesis, device fabrication, and chemical sensing. *Chem. Soc. Rev.* **2013**, *42*, 89–96. [CrossRef] [PubMed]
14. Zheng, Y.; Zhou, T.; Zhang, C.; Mao, J.; Liu, H.; Guo, Z. Boosted charge transfer in SnS/SnO_2 heterostructures: Toward high rate capability for sodium-ion batteries. *Angew. Chem. Int. Ed.* **2016**, *55*, 3408–3413. [CrossRef]
15. Zhang, S.X.; Zhao, Y.J.; Zhang, Q.Y.; Wang, K.J.; Han, J.B. Hollow ZIF-67-C/LDO core/shell heterostructure as a high-performance anode material for sodium ion batteries. *Mater. Lett.* **2021**, *294*, 129817. [CrossRef]
16. Xu, Q.; Li, J.Y.; Sun, J.K.; Yin, Y.X.; Wan, L.J.; Guo, Y.G. Watermelon-inspired Si/C microspheres with hierarchical buffer structures for densely compacted lithium-ion battery anodes. *Adv. Energy Mater.* **2017**, *7*, 1601481. [CrossRef]
17. Jiang, Y.; Song, Y.; Pan, Z.; Meng, Y.; Jiang, L.; Wu, Z.; Yang, P.; Gu, Q.; Sun, D.; Hu, L. Rapid amorphization in metastable $CoSeO_3 \cdot H_2O$ nanosheets for ultrafast lithiation kinetics. *ACS Nano* **2018**, *12*, 5011–5020. [CrossRef]
18. Park, G.D.; Hong, J.H.; Choi, J.H.; Lee, J.H.; Kim, Y.S.; Kang, Y.C. Synthesis process of $CoSeO_3$ microspheres for unordinary Li-ion storage performances and mechanism of their conversion reaction with Li ions. *Small* **2019**, *15*, 1901320. [CrossRef]

19. Park, G.D.; Kang, Y.C. Amorphous cobalt selenite nanoparticles decorated on a graphitic carbon hollow shell for high-rate and ultralong cycle life lithium-ion batteries. *ACS Sustain. Chem. Eng.* **2020**, *8*, 17707–17717. [CrossRef]
20. Iasir, A.R.; Lombardi, T.; Lu, Q.; Mofrad, A.M.; Vaninger, M.; Zhang, X.; Singh, D.J. Electronic and magnetic properties of perovskite selenite and tellurite compounds: $CoSeO_3$, $NiSeO_3$, $CoTeO_3$, and $NiTeO_3$. *Phys. Rev. B* **2020**, *101*, 045107. [CrossRef]
21. Charykova, M.V.; Krivovichev, V.G.; Lelet, M.I.; Yakovenko, O.S.; Suleimanov, E.V.; Depmeier, W.; Semenova, V.V.; Zorina, M.L. A calorimetric and thermodynamic investigation of the synthetic analogs of cobaltomenite, $CoSeO_3 \cdot 2H_2O$, and ahlfeldite, $NiSeO_3 \cdot 2H_2O$. *Am. Mineral.* **2014**, *99*, 742–748. [CrossRef]
22. Yu, S.; Ng, V.; Wang, F.; Xiao, Z.; Li, C.; Kong, L.B.; Que, W.; Zhou, K. Synthesis and application of iron-based nanomaterials as anodes of lithium-ion batteries and supercapacitors. *J. Mater. Chem. A* **2018**, *6*, 9332–9367. [CrossRef]
23. Roy, P.; Srivastava, S.K. Nanostructured anode materials for lithium ion batteries. *J. Mater. Chem. A* **2015**, *3*, 2454–2484. [CrossRef]
24. Chen, M.; Yu, C.; Liu, S.H.; Fan, X.M.; Zhao, C.T.; Zhang, X.; Qiu, J.S. Micro-sized porous carbon spheres with ultra-high rate capability for lithium storage. *Nanoscale* **2015**, *7*, 1791–1795. [CrossRef]
25. Xu, J.M.; He, L.; Xu, W.; Tang, H.B.; Liu, H.; Han, T.; Zhang, C.J.; Zhang, Y.H. Facile synthesis of porous $NiCo_2O_4$ microflowers as high-performance anode materials for advanced lithium-ion batteries. *Electrochim. Acta* **2014**, *145*, 185–192. [CrossRef]
26. Zhong, X.B.; Huang, T.T.; Liang, J.F.; Li, S.X.; Zhang, H.H.; Liu, G.Y.; Wang, G.M. Porous $TiNb_2O_7$@N-C as anode materials for lithium-ion batteries with ultrahigh-rate performance. *J. Phys. Chem. C* **2021**, *125*, 23960–23967. [CrossRef]
27. Zhong, X.B.; Wang, H.Y.; Yang, Z.Z.; Jin, Z.Z.; Jiang, Q.C. Facile synthesis of mesoporous $ZnCo_2O_4$ coated with polypyrrole as an anode material for lithium-ion batteries. *J. Power Sources* **2015**, *296*, 298–304. [CrossRef]
28. Zhang, J.L.; Du, C.F.; Zhao, J.; Ren, H.; Liang, Q.H.; Zheng, Y.; Madhavi, S.; Wang, X.; Zhu, J.W.; Yan, Q.Y. $CoSe_2$-decorated $NbSe_2$ nanosheets fabricated via cation exchange for Li storage. *ACS Appl. Mater. Inter.* **2018**, *10*, 37773–37778. [CrossRef]
29. Hong, L.; Ju, S.L.; Yang, Y.H.; Zheng, J.N.; Xia, G.L.; Huang, Z.G.; Liu, X.Y.; Yu, X.B. Hollow-shell structured porous $CoSe_2$ microspheres encapsulated by MXene nanosheets for advanced lithium storage. *Sustain. Energy Fuels* **2020**, *4*, 2352–2362. [CrossRef]
30. Hu, X.J.; Liu, X.J.; Chen, K.; Wang, G.; Wang, H. Core-shell MOF-derived N-doped yolk-shell carbon nanocages homogenously filled with ZnSe and $CoSe_2$ nanodots as excellent anode materials for lithium- and sodium-ion batteries. *J. Mater. Chem. A* **2019**, *7*, 11016–11037. [CrossRef]
31. Wang, K.; Wang, Y.P.; Zhang, Y.F.; Liu, F.; Shi, J.R.; Liu, S.Y.; Xie, X.F.; Cao, G.Z.; Pan, A.Q. Bimetallic organic framework derivation of three dimensional and heterogeneous metal selenides/carbon composites as advanced anodes for lithium-ion batteries. *Nanoscale* **2020**, *12*, 12623–12631. [CrossRef] [PubMed]
32. Wang, G.Y.; Zhang, M.; Deng, Z.P.; Zhang, X.F.; Huo, L.H.; Gao, S. Poplar branch bio-template synthesis of mesoporous hollow Co_3O_4 hierarchical architecture as an anode for long-life lithium ion batteries. *Ceram. Int.* **2020**, *46*, 29033–29040. [CrossRef]
33. Feng, Y.; Cao, C.Y.; Zeng, J.; Wang, R.C.; Peng, C.Q.; Wang, X.F. Hierarchical porous Co_3O_4 spheres fabricated by modified solvothermal method as anode material in Li-ion batteries. *Trans. Nonferrous Met. Soc. China* **2022**, *32*, 1253–1260. [CrossRef]
34. Zhang, K.; Park, M.; Zhou, L.; Lee, G.H.; Li, W.; Kang, Y.M.; Chen, J. Urchin-like $CoSe_2$ as a high-performance anode material for sodium-ion batteries. *Adv. Funct. Mater.* **2016**, *26*, 6728–6735. [CrossRef]
35. Shen, L.F.; Yu, L.; Yu, X.Y.; Zhang, X.J.; Lou, X.W. Self-templated formation of uniform $NiCo_2O_4$ hollow spheres with complex interior structures for lithium-ion batteries and supercapacitors. *Angew. Chem. Int. Ed.* **2015**, *54*, 1868–1872. [CrossRef]
36. Park, G.D.; Lee, J.K.; Kang, Y.C. Electrochemical reaction mechanism of amorphous iron selenite with ultrahigh rate and excellent cyclic stability performance as new anode material for lithium-ion batteries. *Chem. Eng. J.* **2020**, *389*, 124350. [CrossRef]
37. Park, G.D.; Yang, S.J.; Lee, J.H.; Kang, Y.C. Investigation of binary metal (Ni, Co) selenite as Li-ion battery anode materials and their conversion reaction mechanism with Li ions. *Small* **2019**, *15*, 1905289. [CrossRef] [PubMed]
38. Zhang, N.; Deng, T.; Zhang, S.; Wang, C.; Chen, L.; Wang, C.; Fan, X. Critical review on low-temperature Li-ion/metal batteries. *Adv. Mater.* **2022**, *34*, 2107899. [CrossRef]
39. Huang, Q.; Yang, Z.; Mao, J. Research progress on the low-temperature electrochemical performance of $Li_4Ti_5O_{12}$ anode material. *Ionics* **2017**, *23*, 803–811. [CrossRef]
40. Hu, B.; Zhou, X.; Xu, J.; Wang, X.; Yuan, N.; Ge, S.; Ding, J. Excellent rate and low temperature performance of lithium-ion batteries based on binder-free $Li_4Ti_5O_{12}$ electrode. *ChemElectroChem* **2020**, *7*, 716–722. [CrossRef]